Falter, D., Schröter, K., Nguyen, D., Vorogushyn, S., Kreibich, H., Hundecha, Y., Apel, H., Merz, B. (2015): Spatially coherent flood risk assessment based on long-term continuous simulation with a coupled model chain. - *Journal of Hydrology*, *524*, p. 182-193.

DOI: http://doi.org/10.1016/j.jhydrol.2015.02.021

Spatially coherent flood risk assessment based on long-term continuous simulation with a coupled model chain

Daniela Falter[1], Kai Schröter[1], Nguyen Viet Dung[1], Sergiy Vorogushyn[1], Heidi Kreibich[1], Yeshewatesfa Hundecha[2], Heiko Apel[1], Bruno Merz[1]

[1]GFZ German Research Centre for Geosciences, Section 5.4: Hydrology, Telegrafenberg, Potsdam, Germany

[2]Swedish Meteorological and Hydrological Institute (SMHI), Hydrology Research, Sweden

Correspondence

Daniela Falter, GFZ German Research Centre for Geosciences, Section 5.4: Hydrology, Telegrafenberg, 14473 Potsdam, Germany

Email: falter@gfz-potsdam.de, Phone Number: +49 331 288-1501

Abstract

A novel approach for assessing flood risk in river catchments in a spatially consistent way is presented. The approach is based on a set of coupled models representing the complete flood risk chain, including a multisite, multivariate weather generator, a hydrological model, a coupled 1D-2D hydrodynamic model and a flood loss model. The approach is exemplarily developed for the meso-scale Mulde catchment in Germany. 10,000 years of meteorological fields at daily resolution are generated and used as input to the subsequent models, yielding 10,000 years of spatially consistent river discharge series, inundation patterns and damage values. This allows estimating flood risk directly from the simulated damage. The benefits of

the presented approach are: (1) In contrast to traditional flood risk assessments, where homogenous return periods are assumed for the entire catchment, the approach delivers spatially heterogeneous patterns of precipitation, discharge, inundation and damage patterns which respect the spatial correlations of the different processes and their spatial interactions. (2) Catchment and floodplain processes are represented in a holistic way, since the complete chain of flood processes is represented by the coupled models. For instance, the effects of spatially varying antecedent catchment conditions on flood hydrographs are implicitly taken into account. (3) Flood risk is directly derived from damage yielding a more realistic representation of flood risk. Traditionally, the probability of discharge is used as proxy for the probability of damage. However, non-linearities and threshold behaviour along the flood risk chain contribute to substantial variability between damage probabilities and corresponding discharge probabilities.

Keywords

flood risk analysis, risk model chain, floodplain inundation, continuous simulation

1. Introduction

River flooding is increasingly seen from the risk perspective which considers not only the flood hazard, e.g. discharge and inundation extent, but also the vulnerability and adaptive capacity of the flood-prone regions (Merz et al. 2010). This shift in perspective is visible, for instance, by the development of flood risk maps demanded by the European Flood Directive on the Assessment and Management of Flood Risks (European Commission 2007). These maps are now widely available throughout Europe and are important for risk communication and integrated flood risk management. Alfieri et al. (2013) argued, however, that these maps are generated with inconsistent methods on different spatial scales, using different data bases, and are therefore not comparable on the European scale. Even within European

50 member states, methods might not be consistent, as it is the case for Germany where
51 different federal states adopted different approaches for deriving and presenting flood maps
52 (see e.g. BfG (2014) for an overview). To enable comparisons, Alfieri et al. (2013) proposed
53 the development of a pan-European flood hazard map with a spatial consistent methodology
54 based on the assessment of uniform 100-year flood flows for all river stretches and piece-
55 wise hydraulic modelling of corresponding flood areas.

56 This proposal alleviates the problem of method and data inconsistency, but it does not
57 overcome the problem of assuming spatially uniform return periods for flood scenarios. This
58 traditional approach in flood risk assessment derives scenarios with a constant T-year return
59 period (e.g. T=100) for flood peaks within the entire catchment. The assumption of spatially
60 uniform return periods is valuable for local hazard and risk assessments, however, it is of
61 limited use for large-scale assessments, for example, for national risk policy developments,
62 for large-scale disaster management planning, and in the (re-)insurance industry. The
63 assumption of a T-year flood peak for the entire river network gives an unrealistic large-scale
64 picture. It is not realistic that a single flood reaches a 100-year return period in the entire
65 large-scale river network. Flood risk would be overestimated, as the probability of a single
66 flood reaching a 100-year return period throughout the catchment is much smaller than the
67 probability of a 100-year flood at a single site. The overestimation of flood risk, derived with
68 the traditional approach, was recently shown by Thieken et al. (2014) for the river Rhine in
69 Germany.

70 There are different possibilities for generating flood events that respect the spatial variability
71 of occurrence probability at the catchment scale. One approach that has recently gained
72 attention is the application of multivariate distribution functions to represent the joint
73 probability of flood peaks at multiple sites (e.g. Lamb et al. 2010, Ghizzoni et al. 2012, Keef
74 et al. 2013). A multivariate distribution function, considering the spatial dependence between
75 gauging stations, is fitted to observed flood peaks at multiple gauges and can be used to
76 generate spatial fields of flood peaks. A disadvantage of this method is that only flood peaks

77 are provided. It is not obvious how such an event set could be used as input into unsteady
78 inundation models, because hydraulic models require the entire hydrographs conserving
79 flood volume in order to simulate the temporal evolution of flood waves within the river
80 system. This problem can be bypassed when the event generation starts with the
81 precipitation event. Rodda (2001) developed a stochastic model generating rainfall events for
82 the UK. These events were used as input into a hydrological model to simulate the spatial
83 distribution of the T-year discharge. A disadvantage of the event based simulation approach
84 is the assumption that the return period of flood discharge equals the return period of rainfall.
85 This is usually not given, since storm characteristics, such as the rainfall time pattern, or the
86 initial catchment state influence the relationship between rainfall probability and flood
87 probability (Haberlandt et al. 2014).

88 This simplifying assumption can be avoided by continuous hydrological simulation (e.g.
89 Boughton and Droop 2003, Viviroli et al. 2009, Grimaldi et al., 2013, Haberlandt et al. 2014).
90 This increasingly popular concept consists of generating long synthetic meteorological time
91 series and using them as input into a continuous hydrological model. Flood probabilities can
92 then be derived from the simulated synthetic discharge time series. This approach has the
93 advantage that the complete flood event, including antecedent processes, are modelled
94 throughout the entire catchment in a consistent way. The importance of initial catchment
95 conditions for the flood development was recently investigated by Nied et al. (2013) and also
96 could be observed from the disastrous flood event in 2013 in Central Europe, where the
97 interplay of event precipitation and very wet initial catchments played a dominant role for the
98 exceptional event severity (Schröter et al. 2014). Grimaldi et al. (2013) demonstrated the
99 effect of a continuous hydrologic-hydraulic simulation on floodplain inundation patterns
100 compared to an event-based approach for a small-scale basin.

101 In this paper we extend the ‘derived flood *frequency* approach based on continuous
102 simulation’. By using the synthetic discharge time series as input into flood impact models
103 and deriving flood risk directly from the resulting synthetic damage time series, we propose a

104 novel concept for assessing flood risks: the ‘derived flood *risk* approach based on continuous
105 simulation’. In this way, the processes, and their space-time interactions, underlying the flood
106 risk in a catchment are represented in a consistent way. For instance, simulation of floodplain
107 processes, such as storage effects or channel-floodplain interactions, by hydrodynamic
108 models allows taking into account the effects of floodplain processes on flood damage
109 patterns.

110 A further advantage of implementing a continuous simulation approach is that flood risk can
111 be directly derived from the synthetic damage time series. The return period of damages is
112 thus based on the empirical distribution constructed from long-term simulation. Ideally, risk is
113 estimated as (probability x damage), whereas probability is the probability of damage.
114 Thieken et al. (2014) used this approach by generating a stochastic flood event set from
115 discharge station data, combining it with a flood impact model and fitting an extreme value
116 distribution directly to the synthetic damage data. This attempt to derive flood risk directly
117 from the probability of damage is a rare exception in the flood risk literature. The usual way is
118 to use the probability of discharge or the probability of precipitation as proxy for the
119 probability of damage. However, the probability for the different phenomena (precipitation –
120 discharge – inundation – damage) may change along the flood risk chain. For example, two
121 events with the same flood peak discharge may lead to very different inundation and damage
122 patterns.

123 In this paper, we explore the idea ‘derived flood *risk* approach based on continuous
124 simulation’. The Mulde catchment, a meso-scale catchment in East Germany, is selected as
125 example. A multisite, multivariate weather generator is linked to the Regional Flood Model
126 (RFM). RFM is a coupled model chain, consisting of a continuous hydrological model, 1D/2D
127 hydrodynamic models and a flood loss model. It has been recently developed for risk
128 assessments in large-scale river catchments (Falter et al. 2014). RFM is driven by synthetic
129 meteorological data, generated by a multisite, multivariate weather generator, providing 100
130 realizations of 100 years of data. This virtual period of 10,000 years is simulated

continuously, providing a sample of more than 2,000 flood events with detailed information on inundation depth, extent and damage on a resolution of 100 m. On basis of this unique data set, we present a flood risk analysis directly on damage values. Additionally, this allows us to examine the assumption that probability of peak discharge is a suitable proxy for probability of damage. Derived damage probabilities are compared to corresponding flood peak probabilities to discuss problems that may arise from transformations of flood peak probabilities to damage probabilities.

2. Methods

2.1. Weather Generator

The meteorological input data for the model chain is provided by a multisite, multivariate weather generator (Hundecha and Merz 2012), further advanced from (Hundecha et al. 2009). It provides spatially consistent realisations of meteorological fields for large-scale basins. The model generates synthetic daily meteorological forcing in two stages. In the first stage, precipitation series are generated at multiple sites by respecting the spatial and temporal correlations of the observed daily precipitation amounts on monthly basis. At each station, daily precipitation is sampled from a parametric distribution, which is estimated from the observed daily precipitation series as a mixture of Gamma and Generalized Pareto distributions. The mixing weight varies dynamically with respect to the precipitation intensity. The second stage of the model simulates daily maximum, minimum and average temperatures and solar radiation by keeping the correlations between the variables as well as their inter-site correlation and the autocorrelation of each variable. Temperature values are sampled from Gaussian distributions fitted to the corresponding observations, while for solar radiation a square root transformation was used prior to fitting a Gaussian distribution. Both temperature and solar radiation are conditioned on the state of precipitation. A multivariate autoregressive model is implemented to simulate the time series of all the daily

forcing variables (precipitation, temperature and radiation). Details of the model are presented in Hundecha et al. (2009) and Hundecha and Merz (2012).

2.2. Regional Flood Model RFM

The Regional Flood Model (RFM) is a process-based model cascade developed for flood risk assessments of large-scale basins (Falter et al. 2014). It has been developed for basin areas in the order of several 10,000 km^2. RFM consists of four coupled models: the rainfall-runoff model SWIM, a 1D channel routing model, a 2D hinterland inundation model and the flood loss estimation model for residential buildings FLEMOps+r (Figure 1). We briefly describe the model chain and each model part here, for detailed information the reader is referred to Falter et al. (2014).

2.2.1. Rainfall-runoff model SWIM

The eco-hydrological model SWIM (Soil and Water Integrated Model**,** Krysanova et al. 1998) is a conceptual, semi-distributed model that simulates the hydrological cycle on a daily basis. The model is spatially disaggregated on three levels: The primary unit is the river basin that is subdivided into subbasins and these are further disaggregated into hydrotopes. Water fluxes are computed for each hydrotope and aggregated on the subbasin scale. Computed daily runoff is routed from subbasin to subbasin using the Muskingum hydrological routing scheme. The routed discharges provide a boundary condition for the 1D hydrodynamic river network model.

2.2.2. Hydrodynamic models

The hydrological routing method integrated in SWIM routes the flow on a subbasin scale without considering explicitly the river channel geometry. However, for the prediction of flood defence overtopping and simulation of inundation processes in the hinterland, it is crucial to obtain water level information along the river network. Therefore, a 1D hydrodynamic channel routing model was developed to complement the SWIM routing. Additionally, a 2D hydrodynamic inundation model was implemented to simulate floodplain inundation

processes. Both models are two-way coupled and exchange water level information during runtime.

The developed channel routing model solves a 1D representation of the diffusive wave equations with an explicit finite difference solution scheme. The diffusive wave equation is derived from the full dynamic shallow water equation by neglecting the local and advective acceleration terms. Due to the lack of precise information on the full cross-section geometry and in order to reduce the model run-times, the 1D hydrodynamic river network model only simulates flows exceeding bankfull discharge. The latter is assumed to be equivalent to a 2-year flood derived from the discharge series from the hydrological model at subbasin scale. Runoff time series at each SWIM subbasin outlet are used as boundary condition for the channel routing model. In case the bankfull flow threshold is exceeded within a subbasin, the excess flow is routed downstream subbasin-wise taking the new boundary condition from SWIM at each subbasin outlet into account. The cross-sections representing channel geometry are considered to cover the entire floodplain between flood protection dikes stretching from crest to crest. Whenever a dike crest height is exceeded, outflow into the hinterland is calculated with the broad-crested weir equation.

The dike overtopping discharge is treated as a point source boundary condition for the 2D floodplain model. The outflow of the 1D model is additionally controlled by the feedback of the 2D model. In case the water level in the hinterland is equal to the channel water level, the outflow into the hinterland is stopped. In that way, the uncontrolled water flux out of the 1D model domain is prevented in case the water level in the hinterland exceeds the channel water level.

The 2D inundation model uses a raster-based inertia formulation (Bates et al., 2010) implemented in the CUDA Fortran environment (PGI, Lake Oswego, Oregon, USA) which enables the application on the highly parallelised NVIDIA Graphical Processor Units (GPU; NVIDIA, Santa Clara, California, USA) with a strong performance gain compared to a CPU-based version. The model was benchmarked against a 2D fully dynamic shallow water

model, regarding sensitivity of model performance and run-times to grid resolution (Falter et al. 2013).

For each flood event, where dike overtopping discharge and hinterland inundation occurred, grids of maximum water levels at each cell are extracted and used for calculation of flood loss with a multi-parametric damage model. A flood event starts as soon as bankfull discharge is exceeded anywhere along the river network and ends as soon as discharge drops below bankfull discharge along the whole river.

2.2.3. Flood loss model FLEMOps+r

From the maximum water level grids, damage to residential buildings is calculated for each flood event with the Flood Loss Estimation MOdel for the private sector (FLEMOps+r, Elmer et al. 2010, 2012), developed at the German Research Centre for Geosciences (GFZ), Potsdam. It uses a rule-based multifactorial approach to estimate direct economic damage to residential buildings. The base model version FLEMOps calculates the damage ratio for residential buildings using five different classes of inundation depth, three individual building types, two classes of building quality, three classes of contamination and three classes of private precaution (Thieken et al. 2008). The advanced model version FLEMOps+r additionally considers the return period of the inundation at the affected residential building as an important damage influencing factor (Elmer et al. 2010). Within the RFM framework, FLEMOps+r is applied according to Elmer et al. (2012) without taking into account the influence of precautionary measures and contamination.

3. Application to the Mulde Catchment

3.1. Study Area

The Mulde catchment comprises the Vereinigte Mulde – a sinistral tributary to the Elbe River, and its main frontal flows Zwickauer Mulde, Freiburger Mulde and Zschopau (Figure 2). The total catchment area is approximately 7,400 km^2 (IKSE, 2005). About 70 % of the catchment is dominated by mountain areas that drain a large part of the Ore Mountains, 30 % of the catchment are lowland areas. The elevation ranges from 52 m to 1213 m a.s.l. The mean annual precipitation is about 770 mm, ranging from 1000 mm in the mountains to 550 mm in the lowlands.

The catchment was affected by several severe flood events during the last 100 years: 1954, 1958 2002 (Petrow et al. 2007) and most recent in June 2013. The floods in July 1954, August 2002 and June 2013 were caused by intense and widespread precipitation. The flood in 2013 was additionally triggered by extraordinary initial wetness within the affected basins (Schröter et al. 2014). The August flood in 2002, mainly affecting the Elbe and Danube catchments, was the most expensive natural hazard that occurred in Germany so far and caused damage of around €15 billion in Germany alone (in values of 2013, Merz et al. 2014). The exceptional flood in June 2013 caused about €8.8 billion (Bundestag, 2013; GDV, 2013), although it was more severe in hydrological sense, i.e. with the highest degree of affected river network (Schröter et al. 2014).

For this study, we selected river reaches of the Mulde catchment that have a drainage area larger than 600 km^2 and are located downstream of reservoirs. The final study area comprises about 6,000 km^2 catchment area and about 380 river kilometres (Figure 2).

3.2. Model Set-up

The recent proof-of-concept study by Falter et al. (2014) applied the RFM model chain to the Elbe catchment (Germany) and demonstrated that flood risk assessment based on a continuous simulation approach, including rainfall-runoff, hydrodynamic and damage estimation models is feasible for large catchments. The study revealed however significant

uncertainties especially associated with the 1D hydrodynamic model resulting from channel geometries. Therefore, an advanced set-up of the hydrodynamic models was implemented for the Mulde catchment based on high-resolution topography data.

Daily meteorological input data for 10,000 years were provided by the weather generator for the entire Elbe catchment. The long-term simulation of meteorological fields reflects the climatology from 1951 until 2003 and is assumed to provide a basis for estimating the current flood risk. Likewise, rainfall-runoff simulations with SWIM were performed for the entire Elbe catchment including parts belonging to the Czech Republic. Hydrodynamic models and the flood loss model FLEMOps+r were run only for the proposed study area of the Mulde catchment and were based on the most recent data on river system, dike geometry, topography, land use and building characteristics thus reflecting the present level of flood risk. Data used for flood damage estimation reflects the state as of 2010.

3.2.1. Rainfall-runoff model SWIM

For setting-up the semi-distributed model SWIM, the Elbe catchment was subdivided into 2,268 subcatchments based on the SRTM digital elevation data. The historical hydrometerological input data for SWIM calibration/validation and for parameterisation of the weather generator were provided by the German Weather Service (DWD) from all available stations within Germany and from the Czech Hydrometeorological Institute (CHMI) from stations within the Czech Republic. In addition to the hydrometeorological data, soil and land-use data were derived from the soil map for Germany (BÜK 1000 N2.3), obtained from Bundesanstalt für Geowissenschaften und Rohstoffe (BGR) and the European Soil Database map, obtained from the European Commission's Land Management and Natural Hazards unit and the CORINE (COoRdinated INformation on the Environment) land cover map. SWIM was run with historical daily input data and calibrated over the period from 1981 to 1989. A nested and automatic calibration technique was used in this work by employing the SCE-UA algorithm (Duan et al. 1992). A modified Nash–Sutcliffe efficiency (mNS) presented as

normalised weighted sum of the squared differences between the observed and simulated discharges was employed as an objective function (Hundecha and Bárdossy 2004) giving more emphasis to higher flows:

$$mNS = 1 - \frac{\sum_{i=1}^{N} w(\cdot)(Q_c(t_i) - Q_0(t_i))^2}{\sum_{i=1}^{N} w(\cdot)(Q_0(t_i) - \bar{Q}_0)^2} \quad [1]$$

where $Q_c(t_i)$ and $Q_0(t_i)$ are the simulated and observed discharges at time t_i, respectively, and Q_0 is the mean observed discharge over the simulation period (N days), $w(\cdot)$ is a weight which is equal to the observed discharge $Q_0(t_i)$.

3.2.2. Hydrodynamic models

To simulate water levels along the selected river network with the 1D hydrodynamic river network model, the following input data is needed: river cross-section profiles, dike location and height information, Manning's roughness values and boundary conditions (Figure 1). The main data source for the acquisition of river cross-section profiles including dike location and elevation along the river network was a digital elevation model (DEM) with 10-m horizontal resolution, provided by the Federal Agency for Cartography and Geodesy in Germany (BKG), with a vertical accuracy of ± 0.5–2 m. Additional information on dike location and channel width were taken from the digital basic landscape model (Base DLM) also provided by the BKG. Profiles were manually extracted in 500 m distance, perpendicular to the flow direction, with the GIS integrated tool Hec-GeoRas 10 for ArcGIS 10 (US Army Corps of Engineers, May 2012). Since only overbank flow above threshold was routed by 1D model, cross-section profiles were corrected to represent only active floodplain without river channel. Cross-sections were further simplified to trapezoid-shape, by an algorithm that extracted the necessary parameters (channel location and width, dike location, bottom height of the dike, dike crest height and ground elevation, respectively bankfull depth) while conserving the original cross-section area. Dike heights are not well resolved by the DEM 10. Therefore a minimum dike height of 1.8 m was assumed at dike locations provided by the base DLM. The threshold for bankfull flow was assumed to be equivalent to a 2-year flood (Bradbrook et al.

311 2005, Rodda 2005) and computed from simulated discharge series at each subbasin outlet.
312 The runoff-boundary condition from SWIM assigned to the corresponding cross-section in the
313 1D hydrodynamic model is corrected by subtracting bankfull flow from the total runoff. The
314 Manning's value (n = 0.03) was assumed to be homogenous for the whole river network. In
315 case of dike overtopping, the width of overtopping flow was assumed to be 20 m. The 1D
316 river network model is two-way coupled with the 2D hinterland inundation model and
317 provides computed overtopping flow as boundary condition to the 2D model, while receiving
318 hinterland water levels controlling the channel water level and overtopping flow.

319 The 2D raster-based inertia model was based on the computational grid of 100 m resampled
320 from the DEM 10. The resampling was dictated by computational constrains. The 100m
321 resolution was selected based on the previous benchmark study by Falter et al. (2013), who
322 found this to be a reasonable resolution based on trade-off between computational time and
323 accuracy in terms of predicted inundation areas and depths. The computationally intensive
324 2D modelling was performed only for the hinterland, and the channel and river banks
325 embedded between dikes (1D model domain) were excluded from the 2D modelling domain.
326 This simplification reduced run-time requirements considerably and seems justified for risk
327 assessment studies along diked river stretches in Germany where assets in floodplains
328 between dikes are minor compared to those on protected floodplains. Roughness grid was
329 generated from CORINE land use maps by assigning roughness values from literature
330 (Chow, 1959; Bollrich, 2000) to different land-use classes. The boundary conditions derived
331 from the 1D hydrodynamic channel network model in form of dike crest overtopping flow are
332 assigned to the corresponding cell of the 2D calculation grid by location.

333 ***3.2.3. FLEMOps+r***

334 The estimation of flood damage to residential buildings using FLEMOps+r requires spatially
335 detailed information about asset values, building quality and building type. Inundation depths
336 and return period of peak flows are used as impact variables to evaluate flood loss ratio. All

337 input data in grid format were scaled to a spatial resolution of 100 m to comply with the 2D
338 hydrodynamic modelling output.

339 Asset values of the regional stock of residential buildings are defined on the basis of
340 standard construction costs (BMVBS, 2005), i.e. quantifying the market price of the
341 construction works for restoring a damaged building (Kleist et al. 2006). The values used
342 reflect the state of 2010. The asset values were disaggregated to the digital basic landscape
343 model (Basic DLM) of the German ATKIS (Authoritative Topographic Cartographic
344 Information System; BKG GEODATENZENTRUM 2009) using the binary disaggregation
345 scheme proposed by Wünsch et al. (2009). Within this procedure the ATKIS objects of the
346 'residential areas' (ATKIS code 2111) and 'areas of mixed use' (ATKIS code 2113) are used
347 to determine residential areas.

348 The characteristics of the municipal building stock are derived from the INFAS Geodaten
349 data set (Infas Geodaten GmbH, 2009). The composition of building types in each
350 municipality is described using a cluster centre approach. In total, five clusters are defined
351 differentiating the share of single-family houses, semi-detached/detached and multifamily
352 houses (Thieken et al. 2008). Average building quality is aggregated to two classes; high
353 quality and medium/low quality (Thieken et al. 2008).

354 The spatial distribution of inundation depths is provided by the 2D raster-based inertia model.
355 Maximum inundation depths (h) for different flood events are classified according to the
356 classes defined in the FLEMOps+r model ($0\ m < h \leq 0.2\ m$; $0.2\ m < h \leq 0.6\ m$; $0.6\ m < h \leq$
357 $1.0\ m$; $1.0\ m < h \leq 1.5\ m$; $1.5\ m < h$). Return periods of flood discharge peaks are estimated
358 within each SWIM subbasin on the basis of extreme value statistics (GEV) derived from
359 annual maximum discharge series generated through the long-term (10,000 years)
360 continuous SWIM simulation of the Elbe catchment.

361 The estimation of flood losses comprises the determination of the damage ratio to residential
362 buildings given the inundation depths and return periods, as well as the information about

363 building quality and building type clusters in each location affected by flooding. Absolute
364 flood losses in Euros are calculated as the product of damage ratio and location-dependent
365 asset value per raster cell.

366

367 4. Results and Discussion

368 4.1. RFM Model Performance Evaluation

369 The performance of the coupled model chain was evaluated on the period of 1951-2003
370 where possible with observed data.

371 *4.1.1 Runoff validation*

372 The hydrological model SWIM was calibrated and validated on 20 gauging stations in the
373 entire Elbe catchment, whereas 3 gauging stations were located within the Mulde catchment
374 (Figure 2). The validation was performed for the period 1951-2003 with observed discharge
375 data, excluding the calibration period of 1981-1989. Results indicate a reasonable simulation,
376 especially of high discharges, for the Mulde catchment with mNS larger than 0.8.
377 Additionally, the conventional Nash-Sutcliffe (NS) values are displayed in Table 1 for
378 reference. The results indicate that SWIM is particularly tuned to adequately simulate high
379 flows relevant for flood risk assessment.

380 *4.1.2 Water level evaluation*

381 Water levels simulated by the 1D hydrodynamic model were validated at 5 gauging stations
382 throughout the catchment (Figure 2) with observed water level data for the period of 1951-
383 2003. Peak errors are in the range of 0.18 - 0.56 m (Table 2) and are in the range of
384 uncertainty associated with dike crest heights controlling overtopping flow. As indicated by
385 the bias, both an overall water level under- and overestimation occur likewise. Although dike
386 overtopping is a threshold process sensitive to water level height, we consider the simulation

acceptable for large-scale purposes aiming at providing the large-scale picture but not at representing local details.

4.1.3 Inundation extent evaluation

Evaluation of inundation extent simulations of past floods is difficult, as availability of inundation extents, e.g. from satellite data, is limited. Particularly, in non-natural urbanised floodplains protected by dikes widespread inundations are exceptional and strongly controlled by performance of flood protection structures. In our case only for the flood in August 2002 inundation extents are documented by the National Aeronautics and Space Research Centre of the Federal Republic of Germany (DLR). A comparison of observed and simulated inundation extents is shown in Figure 3. For the Freiberger Mulde, inundated areas match quite well as partly constricted by topographic barriers. For the other parts of the catchment, over- and underestimation of inundated areas are present. Especially for the low-land part of the Vereinigte Mulde inundation patterns are widespread but were not exactly represented by the model resulting in a Flood Area Index (FAI) of 0.49. FAI is defined as follows:

$$FAI = \frac{M1D1}{M1D1+M1D0+M0D1} \quad [2]$$

where, M1D1 is the number of cells correctly predicted as flooded, M1D0 is the number of cells flooded in the prediction and observed dry and M0D1 the number of cells dry in the prediction, however, observed wet. Only about 50% of the flood extent was correctly predicted by the simulation. Flood events at this scale are complex particularly when occurring dike breaches strongly shape inundation extent as was the case in the Mulde catchment in 2002. Within the current version of the hydrodynamic model dike breach processes are not implemented and no detailed information on the time and dynamics of breaching process was available. For large-scale applications, we consider the model to give a reasonable estimate on the dimension of the inundation extent and the severity of the event. Although, a general underestimation of inundation extents is to be expected by disregarding dike breach processes.

4.1.4 Damage estimation evaluation

Official damage estimates for the August 2002 flood are available for all 19 affected communities in the Federal State of Saxony in Germany which can be used to evaluate the results of the FLEMOps+r model. For these communities the sum of damage to residential buildings officially reported for the August 2002 flood (Staatskanzlei Freistaat Sachsen 2003; SAB, personal communication 2004) amounts to €240 million. The results obtained from the model chain in these communities amount to €67 million, which are about 30 % of the reported numbers.

Mainly two factors presumably contribute to this underestimation. First, the differences in inundated areas between the DLR flood footprint and hydraulic model results (FAI=0.49) translates into differences in affected residential areas. According to the DLR flood footprint, 9.9 km² of residential areas have been affected in August 2002 in the study region. The hydraulic model estimated 7.9 km² affected residential areas which amounts about 80%. In addition, the simulated and observed inundation patterns are not exactly matching. The Flood Area Index computed only for residential areas (FAIres), compare Equation 2, for the hydraulic simulation is 0.29. Hence, the simulation correctly predicts about 30% of the affected residential areas. Accordingly, the areas where damage was actually caused by the 2002 flood differ considerably from the simulation. Therefore, the comparison of the damage values should be interpreted with caution. Second, former applications of FLEMOps+r on the meso-scale indicate a tendency to underestimate damage, e.g. (Wünsch et al. 2009, Jongman et al. 2012). In this light, the systematic underestimation of reported damage may be also due to uncertainty in asset values and their spatial distribution and/or to the uncertainty of the damage model.

4.2 Long-term Simulation Results: Flood Risk in the Mulde Catchment

For the continuous and long-term simulation, RFM was driven by meteorological input data, generated by the weather generator. The weather generator was set up to generate synthetic weather variables based on observed meteorological data for the years 1951-2003. Consequently, the weather generator reproduces the climate conditions of this time period. In total, 100 realizations of 100 years of daily weather variables were generated at 528 stations within Germany and neighboring upstream countries. The virtual period of 10,000 years of meteorological data served as input for the RFM. The rainfall-runoff model SWIM, set up for the entire Elbe catchment, was driven by the synthetically generated weather variables to provide daily discharge data on a subbasin scale that subsequently served as input for the hydraulic models. 1D/2D hydrodynamic simulations are extensive in terms of run time, however, could be realized by application on a NVIDIA Tesla C1060 GPU server, containing four devices with each having 240 processor cores. The simulation of the virtual period of 10,000 years for the Mulde catchment took about 10 days run time. In total 2,016 flood events, where hinterland inundation has occurred, were simulated. For each event, damage to residential buildings was calculated with the model FLEMOps+r. This resulted in a unique data set of about 2,000 flood loss events including spatially detailed information on inundation depths and damage to residential buildings that served as basis for the subsequent flood risk analysis.

In Figure 4 we present the total count of flooding events for each computational cell of 100 m resolution. The frequency of flooding is unevenly distributed in space. There are areas that are flooded up to 1,326 times in 10,000 years and others are never affected by inundation. Patterns like that are to be expected, as there are always areas that are more flood prone than others for several reasons. Remarkably, there are no areas inundated in all of the 2,016 flood events. This illustrates that the model chain provides different spatial patterns of flood generation and alternating inundation pathways within the Mulde catchment. As both

tributaries Zwickauer and Freiberger Mulde seem to be affected nearly equally often, this suggests an alternating centre of flood impact between those tributaries.

4.2.1 Flood frequency estimation

The combined performance of the weather generator and SWIM was evaluated by comparing the flood frequency curve derived by simulation with the flood quantiles based directly on observed discharge. Figure 5 shows this comparison for gauge Bad Düben, the most downstream gauge of the Mulde catchment (see Figure 2). For this gauge daily flow was available for the 43-year period 1951-2003. The plotting positions were calculated according to Weibull. The derived flood frequency curve was estimated using the following resampling approach: Annual maximum discharge values were extracted from the 10,000 year continuous simulation. 1,000 random samples of length 43 were drawn with replacement from these 10,000 values, and the Generalised Extreme Value distribution was fitted to each sample. Parameters were estimated via L-moments (Hosking and Wallis, 1997). The median and the 50% and 95% confidence intervals are derived from the 1,000 flood frequency curves.

Figure 5 shows that the derived flood quantiles agree reasonably well with the observation based plotting positions. Two events are clearly outside the 95% sampling uncertainty, namely the floods in 1974 and 2002. These two largest events need to be put in perspective. They resulted from unusually high precipitation amounts in the Ore Mountains, the headwater areas of the Mulde catchment. A total of 312 mm within 24 h was recorded on 12 and 13 August 2002 at Zinnwald. This is the highest amount of rainfall that has ever been measured in Germany (Ulbrich et al. 2003). Given that the rainfall generator has been set up for the much larger Elbe catchment, thereby ignoring some of the local rainfall variability, and the extreme nature of these two events in the Mulde headwater catchments, Figure 5 shows a good agreement between observations and derived flood quantiles.

4.2.2 Flood risk curves

Usually, it is not possible to estimate flood loss probabilities directly from damage data, as information on flood loss is sparse or the number of synthetic event sets is not large enough to draw robust statistics. Here, the number of loss events derived from more than 2000 simulated floods within different subbasins ranges between 0 and 774. Apparently not every flood caused damage in each subbasin. This unique data set allowed for the first time to estimate the probabilities directly from damage data. Flood risk curves were derived for all 19 Mulde subbasins based on the aggregated damage values. However, the estimates for 7 subbasins were excluded from the analysis, as the number of damage events was too small (below 30).

In Figure 6, the histograms of damage values, aggregated to the subbasin level, and the risk curve are displayed for an example subbasin. The step in the risk curve visible for p = 0.99 (100-years return period) results from loss estimates of the FLEMOps+r model. FLOMOps+r uses the recurrence interval of the peak discharge as an explanatory variable on an ordinal scale which defines three different classes (below 10 years, above 10 years and below 100 years, above 100 years). As a consequence, loss estimates increase stepwise at 10 and 100 years causing also shifts in the loss estimate. This threshold behavior implicitly reflects increasing damage propensity in areas which have been affected by low probability events only. This in turn is related to lower flood experiences, lower preparedness and lower resistance, and hence, higher damage (Elmer et al. 2010).

Figure 6a illustrates that the distribution of flood loss is strongly skewed. For the example subbasin, there were 646 loss events during the 10,000 year simulation period. Damage was smaller than 4 million € in 85% (551 events) and smaller than 1 million € in 48% (313 events), however, there were also a few very large loss events with more than 30 million € damage.

To illustrate the advantage of our approach, we compared the risk curves based on our approach and on the traditional approach. In our approach, the probability of a loss event is

517 directly derived from the sample of the damage data (empirical cumulative distribution
518 function CDF in Figure 6b). In contrast, the traditional approach uses the probability of peak
519 discharge as a proxy for damage probability, by fitting a Generalized Extreme Value (GEV)
520 distribution to the simulated annual maximum flows of the 10,000 years period (GEV-based
521 proxy in Figure 6b). Probabilities of peak flows scatter in varying degree around the loss
522 probabilities (note the log scale of the y-axis). This highlights the strong variability in the
523 relationship between probability of peak runoff and probability of damage.

524 ***4.2.3 Is probability of peak runoff a suitable proxy for probability of damage?***

525 As discussed before, the probability of damage is commonly approximated by the probability
526 of peak runoff as information on flood loss is rare. This approximation is based on the
527 assumption that there is an unambiguous transformation between these probabilities. This
528 assumption holds on average for individual subbasins, however, Figure 5b illustrates that
529 there is significant variability around the mean behaviour, and that the return period of runoff
530 peaks does not necessarily increase with increasing damage. For example, events in the
531 range of 800 years return period may cause damage between 1.5 and 2.5 million €. Similarly,
532 a loss event of 1.2 million € may be caused by events with return periods between 120 and
533 400 years.

534 To illustrate this observation, we selected two flood events with the same peak runoff but
535 different damage. One simulation caused 122,058 € damage within the subbasin 995,
536 whereas another one almost the double loss of 236,935 €. The return period of the
537 corresponding peak flow was about T= 50 years. Although the peak runoff is the same, the
538 shape of the hydrographs is different. The second flood featured a larger volume. When
539 dikes are overtopped, this caused a larger volume of water flowing into the hinterland and,
540 hence, higher inundation depth with differences up to 2.7 m (Figure 7) and higher damages.
541 Of course, there are also examples where floods with different runoff peaks result in the
542 same damage. For example, two simulations resulted in a damage of 2,791,450 € within

543 subbasin 1012, while the peak runoffs corresponded to T = 86 years and T = 51 years,
544 respectively.

545 A flood loss event is the outcome of complex interactions along the flood risk chain, from the
546 flood-triggering rainfall event through the processes in the catchment and river system, the
547 behaviour of flood defences, the spatial patterns of inundation processes, the superposition
548 of inundation areas with exposure and flood damaging mechanisms. Hence, the common
549 assumption that peak runoff corresponds proportionally to damage is not necessarily valid.
550 The presented long-term, continuous simulation of the complete flood risk chain proved to be
551 capable of partly representing these process interactions. Not represented by our current
552 model setup, however, are dike breach processes and subsequent flood attenuation and
553 storage effects. In case of a dike breach, the relationship between peak runoff and damage
554 is all the more questionable. This is the case for the dike breach location, but also for the
555 downstream part of the river. In case dike breach effects are represented it is to expect that
556 differences in discharge probabilities and loss probabilities increase.

557 Our results show the discrepancy in traditional flood risk estimates, whereas risk is based on
558 the probability of peak discharge, and the more comprehensive approach, where risk is
559 based on the probability of damage. Relying on return periods of maximum flows may result
560 in both under- and overestimation of risk values.

561 ### *4.2.4 Spatial flood risk patterns and their variability*

562 The presented coupled model chain allows deriving spatially consistent flood risk estimates
563 at any scale – from the local scale to the catchment scale. Figure 8a shows, for example, the
564 distribution of the expected annual damage (EAD) as risk indicator at the subbasin scale.
565 The EAD values differ between subbasins, highlighting the spatial variability in both flood
566 hazard (discharge, inundation extent and depth) and vulnerability (exposure, susceptibility).

567 Figure 8b to 8e compare the spatial distribution of discharge return periods and flood
568 damage for two exemplary sets of flood events in the Mulde catchment with approximately

28 and 68 million Euro damage, respectively. Single flood events exhibit a strong variability of discharge return periods (more than two orders of magnitude) across different subbasins opposed to the steady values of damage return period of 114 yr (standard deviation of damage return periods: σ = 2.4 yr) and 238 yr (σ = 5.67 yr). This highlights the importance of explicitly considering the spatial variability of flood hazard contrary to the assumption of homogeneous return periods for large-scale basins.

The results further point out the presence of non-linear or threshold processes in the relationship between discharge return period and damage. For instance in subbasin 994 (Figure 8b-e), the damage value increases disproportionally above the return period of about 50 years. This can be a result of the dike overtopping process and/or jump in the affected assets. Furthermore, the order of flood events according to the discharge return period does not necessarily translates into the order of damage values as shown for subbasin 1012 (Figure 8b-e). This highlights the importance of different inundation pathways affecting spatially distributed assets in various manners with increasing flood hazard. These pathways can be shaped by both the flood generation processes, reflected in the flood wave form, and by river and floodplain processes such as dike overtopping and inundation front propagation patterns. Once again, the return period of discharge attached to an entire subbasin is not capable of fully explaining the variability of damage and serving as a robust proxy for damage probability. This advocates our spatially distributed and continuous simulation approach to obtain spatially consistent distributed risk values. Assuming a homogeneous discharge return period across all subbasins as in the traditional risk assessment approach would also lead to a spatially distributed pattern of EAD values. Those would be, however, conditioned only by the spatial variability in vulnerability and neglect the spatial variability of hazard.

5 Conclusions

This paper presents a novel approach for assessing flood risk in river catchments in a spatially consistent way. The derived flood risk approach is based on a set of coupled

models representing the complete flood risk chain, including a large-scale multisite, multivariate weather generator, a hydrological model, a coupled 1D-2D hydrodynamic model and a flood loss estimation model. Long time series of spatially consistent meteorological fields are generated and transformed, through the subsequent models, into long time series of flood damage. This allows deriving flood risk estimates directly from the simulated damage.

The approach is exemplarily developed for the meso-scale catchment Mulde, located in Eastern Germany. 10,000 years of spatially consistent meteorological time series are generated and used as input to the model chain, yielding 10,000 years of spatially consistent river discharge series, inundation patterns and damage values. This results in a unique data set of more than 2,000 flood events, including detailed spatial information on inundation depth and damage at a resolution of 100 m. On this basis flood risk curves and risk indicators, such as expected annual damage, can be derived for any scale, from the grid cell scale to the catchment scale. The derived flood risk approach is per se transferable to other river basins without methodological limitations. The selection of models to simulate flood risk chain processes and case-specific hydro-meteorological and topographic data will certainly affect the accuracy of resulting risk estimates.

To the authors' knowledge, this is the first study which extends the derived flood frequency approach based on long-term continuous simulation and computes flood damage and associated risk. We foresee a number of advantages for this approach compared to the traditional flood risk assessments:

(1) Spatially coherent patterns of catchment meteorology, hydrology and floodplain processes:

In contrast to traditional flood risk assessments, where homogenous return periods are assumed for the entire catchment, the presented approach delivers spatially heterogeneous patterns which respect the spatial correlations of the different processes

and their spatial interactions. For example, the spatial correlation structure of rainfall is modelled by the weather generator resulting in consistent event fields. Further, the superposition of flood waves at river confluences as function of rainfall characteristics and initial catchment state is implicitly considered. This advantage is particularly valuable for large-scale assessments, where it cannot be assumed that the catchment is uniformly affected by a single flood event.

(2) Holistic representation of flood processes:

Catchment and floodplain processes are represented in a holistic way, since the complete chain of flood processes is represented by the coupled model approach. For instance, the effects of spatially varying antecedent catchment conditions on the flood hydrographs are implicitly taken into account. Another example is the damage-reducing effect immediately downstream of a river reach where large water volumes overtop the dike. Running the coupled model in the continuous modes implicitly considers such effects. Contrary to the traditional event based approach, it is not necessary to define representative events based on flood frequency analysis and synthetic hydrographs.

(3) More realistic representation of damage probability, and hence, flood risk:

Traditional flood risk assessments use the probability of discharge as proxy for the probability of damage. Our approach of simulating the complete flood risk chain for long periods, e.g. 10,000 years, enables us to derive flood risk directly from damage data and their empirical frequency distribution. Problems associated with translating the probabilities of rainfall or peak runoff to probabilities of damage are bypassed. A comparison of damage probabilities and corresponding discharge probabilities shows a substantial variability in this relationship at the subbasin scale. Non-linearities and threshold behaviour along the flood risk chain contribute to this variability. For example, flood damage depends not only on the flood peak but on the hydrograph shape or floodplain hydraulics including dike overtopping and inundation pathways. Differences in

discharge and damage probabilities are expected to further increase between traditional and derived flood risk approach, when dike breach processes are accounted for in the hydrodynamic modelling.

Acknowledgements

The work reported in this paper is part of the project 'Regional Flood Model for Germany' undertaken at the GFZ German Research Centre for Geosciences. We thank the Federal Agency for Cartography and Geodesy in Germany (BKG) for provision of the digital elevation model of Germany (DGM- D), the German Weather Service (DWD) for providing meteorological data and the authorities that provided gauging station data.

References

Alfieri, L., Salamon, P., Bianchi, A., Neal, J., Bates, P., Feyen, L. (2014). Advances in pan-European flood hazard mapping. *Hydrological Processes*, *28*(13), 4067–4077. doi: 10.1002/hyp.9947

Bates, P. D., Horritt, M. S., Fewtrell, T. J. (2010). A simple inertial formulation of the shallow water equations for efficient two-dimensional flood inundation modelling. *Journal of Hydrology*, *387*(1-2), 33–45. doi: 10.1016/j.jhydrol.2010.03.027

BfG. (2014). Geoportal. Retrieved July 26, 2014, from http://geoportal.bafg.de/mapapps/resources/apps/HWRMRL-DE/index.html?lang=de

BKG GEODATENZENTRUM. (2009). ATKIS-Basis-DLM.

BMVBS. (2005). *Normalherstellungskosten 2005 (NHK 2005)*. Berlin: Bundesministerium für Verkehr, Bau und Stadtentwicklung.

Bollrich, G. (2000). *Technische Hydromechanik*. Berlin: Verlag Bauwesen.

Boughton, W., Droop, O. (2003). Continuous simulation for design flood estimation – a review. *Environmental Modelling and Software*, 18 (49), 309–318.

Bradbrook, K., Waller, S., Morris, D. (2005). National floodplain mapping: datasets and methods –160,000 km in 12 months. *Natural Hazards*, 103–123.

676 Bundestag, D. (2013). *Bericht zur Flutkatastrophe 2013: Katastrophenhilfe, Entschädigung,*
677 *Wiederaufbau*. Berlin.

678 Chow, V. T. (1959). *Open channel Hydraulics*. New York, USA: McGraw-Hill.

679 European Commission (2007). Directive 2007/60/EC of the European Parliament and of the
680 Council of 23 October 2007 on the assessment and management of flood risks. *Off J*
681 *Eur Communities 2007a*, (2455), 27–34.

682 Duan, Q., Sorooshian, S., Gupta, V. (1992). Effective and efficient global optimization for
683 conceptual rainfall-runoff models. *Water Resources Research*, *28*(4), 1015–1031.

684 Elmer, F., Hoymann, J., Düthmann, D., Vorogushyn, S., Kreibich, H. (2012). Drivers of flood
685 risk change in residential areas. *Natural Hazards and Earth System Science*, *12*(5),
686 1641–1657. doi: 10.5194/nhess-12-1641-2012

687 Elmer, F., Thieken, A. H., Pech, I., Kreibich, H. (2010). Influence of flood frequency on
688 residential building losses. *Natural Hazards and Earth System Science*, *10*(10), 2145–
689 2159. doi: 10.5194/nhess-10-2145-2010

690 Falter, D., Dung, N. V., Vorogushyn, S., Schröter, K., Hundecha, Y., Kreibich, H., Apel, H.,
691 Theisselmann, F., Merz, B. (2014). Continuous, large-scale simulation model for flood
692 risk assessments: proof-of-concept. *Journal of Flood Risk Management*, in press. doi:
693 10.1111/jfr3.12105

694 Falter, D., Vorogushyn, S., Lhomme, J., Apel, H., Gouldby, B., Merz, B. (2013). Hydraulic
695 model evaluation for large-scale flood risk assessments. *Hydrological Processes*, *27*(9),
696 1331 – 1340. doi: 10.1002/hyp.9553

697 Ghizzoni, T., Roth, G., Rudari, R. (2012). Multisite flooding hazard assessment in the Upper
698 Mississippi River. *Journal of Hydrology*, 412-413, 101-113, doi:
699 10.1016/j.jhydrol.2011.06.004

700 GDV. (2013). *Erste Schadenbilanz: Hochwasser 2013 verursacht 180.000 versicherte*
701 *Schäden in Höhe von fast 2 Milliarden Euro*. Retrieved from
702 http://www.presseportal.de/pm/39279/2505807/erste-schadenbilanz-hochwasser-2013-
703 verursacht-180-000-versicherte-schaeden-in-hoehe-von-fast-2

704 Grimaldi, S. et al., 2013. Flood mapping in ungauged basins using fully continuous
705 hydrologic–hydraulic modeling. *Journal of Hydrology*, 487, 39–47, doi:
706 10.1016/j.jhydrol.2013.02.023

707 Haberlandt, U., Radtke, I. (2014). Hydrological model calibration for derived flood frequency
708 analysis using stochastic rainfall and probability distributions of peak flows. *Hydrol.*
709 *Earth Syst. Sci*., 18, 353–365, doi: 10.5194/hess-18-353-2014

710 Hosking, J. R. M., Wallis, J. R. (1997). Regional frequency analysis: An approach based on
711 L-moments. Cambridge University Press, Cambridge, UK, 1997, 224 p.

712 Hundecha, Y., Bárdossy, A. (2004). Modeling of the effect of land use changes on the runoff
713 generation of a river basin through parameter regionalization of a watershed model.
714 *Journal of Hydrology*, *292*(1-4), 281–295. doi: 10.1016/j.jhydrol.2004.01.002

715 Hundecha, Y., Merz, B. (2012). Exploring the relationship between changes in climate and
716 floods using a model-based analysis. *Water Resources Research*, *48*(4), W04512, doi:
717 10.1029/2011WR010527

718 Hundecha, Y., Pahlow, M., Schumann, A. (2009). Modeling of daily precipitation at multiple
719 locations using a mixture of distributions to characterize the extremes. *Water Resources*
720 *Research*, *45*(12), W12412, doi: 10.1029/2008WR007453

721 IKSE. (2005). *Die Elbe und ihre Einzugsgebiete*. Magdeburg.

722 Infas Geodaten GmbH. (2009). Infas Geodaten.

723 Jongman, B., Kreibich, H., Apel, H., Barredo, J. I., Bates, P. D., Feyen, L., Ward, P. J.
724 (2012). Comparative flood damage model assessment: towards a European approach.
725 *Natural Hazards and Earth System Science*, *12*(12), 3733–3752. doi: 10.5194/nhess-
726 12-3733-2012

727 Keef, C., Tawn, J. A., Lamb, R. (2013). Estimating the probability of widespread flood events.
728 *Environmetrics*, *24*(1), 13–21. doi: 10.1002/env.2190

729 Kleist, L., Thieken, A. H., Köhler, P., Schroeder [Müller], M., Seifert, I., Borst, D., Werner, U.
730 (2006). Estimation of the regional stock of residential buildings as a basis for a
731 comparative risk assessment in Germany. *Natural Hazards and Earth System Sciences*,
732 6(4), 541-552, doi: 10.5194/nhess-6-541-2006

733 Krysanova, V., Müller-Wohlfeil, D., Becker, A. (1998). Development and test of a spatially
734 distributed hydrological/water quality model for mesoscale watersheds. *Ecological*
735 *Modelling*, *106*, 261–289.

736 Lamb, R., Keef, C., Tawn, J., Laeger, S., Meadowcroft, I., Surendran, S., Batstone, C.
737 (2010). A new method to assess the risk of local and widespread flooding on rivers and
738 coasts. *Journal of Flood Risk Management*, *3*(4), 323–336, doi: 10.1111/j.1753-
739 318X.2010.01081.x

740 Merz, B., J. Hall, M. Disse, A. Schumann (2010) Fluvial flood risk management in a changing
741 world. *Natural Hazards and Earth System Sci*ences, 10, 509–527, doi: 10.5194/nhess-
742 10-509-2010

743 Merz, B., Elmer, F., Kunz, M., Mühr, B., Schröter, K., Uhlemann-Elmer, S. (2014). The
744 extreme flood in June 2013 in Germany. *La Houille Blanche*, *1*(1), 5–10, doi:
745 10.1051/lhb/2014001

746 Nash, J., Sutcliffe, J. (1970). River flow forecasting through conceptual models part I—A
747 discussion of principles. *Journal of Hydrology*, *10*, 282–290.

748 Nied, M., Hundecha, Y., Merz, B. (2013). Flood-initiating catchment conditions: a spatio-
749 temporal analysis of large-scale soil moisture patterns in the Elbe river basin. *Hydrology*
750 *and Earth System Sciences,* 17, 1401-1414, doi: 10.5194/hess-17-1401-2013

751 Petrow, T., Merz, B., Lindenschmidt, K.-E., Thieken, A. H. (2007). Aspects of seasonality and
752 flood generating circulation patterns in a mountainous catchment in south-eastern
753 Germany. *Hydrology and Earth System Sciences*, 11, 1455-1468, doi:10.5194/hess-11-
754 1455-2007

Rodda, H. J. E. (2001). The Development of A Stochastic Rainfall Model for UK Flood Modelling. In P. Krahe, D. Herpertz (Eds.), *Generation of Hydrometeorological Reference Conditions for Assessment of Flood Hazard in large River Basins*. Koblenz.

Rodda, H. J. E. (2005). The Development and Application of a Flood Risk Model for the Czech Republic. *Natural Hazards*, *36*(1-2), 207–220. doi: 10.1007/s11069-004-4549-4

Schröter, K., Kunz, M., Elmer, F., Mühr, B., Merz, B. (2014). What made the June 2013 flood in Germany an exceptional event? A hydro-meteorological evaluation. *Hydrology and Earth System Sciences Discussions*, *11*(7), 8125–8166. doi: 10.5194/hessd-11-8125-2014

Staatskanzlei Freistaat Sachsen. (2003). *Schadensausgleich und Wiederaufbau im Freistaat Sachsen* (p. 126). Dresden: Leitstelle Wiederaufbau.

Thieken, a. H., Apel, H., Merz, B. (2014). Assessing the probability of large-scale flood loss events: a case study for the river Rhine, Germany. *Journal of Flood Risk Management*, in press. doi: 10.1111/jfr3.12091

Thieken, A. H., Olschewski, A., Kreibich, H., Kobsch, S., Merz, B. (2008). Development and evaluation of FLEMOps – a new F lood L oss E stimation MO del for the p rivate s ector. In E. Proverbs, D., Brebbia, C. A., Penning-Rowsell (Ed.), *Flood Recovery, Innovation and Response* (Vol. I, pp. 315–324). Southampton, UK: WIT Press. doi: 10.2495/FRIAR080301

Ulbrich, U., Brücher, T., Fink, A. H., Leckebusch, G. C., Krüger, A., Pinto, J. G. (2003). The Central European Floods in August 2002. Part I: Rainfall periods and flood development. *Weather*, 58(10), 371-377.

Wünsch, A., Herrmann, U., Kreibich, H., Thieken, A. H. (2009). The role of disaggregation of asset values in flood loss estimation: a comparison of different modeling approaches at the Mulde River, Germany. *Environmental Management*, *44*(3), 524–541. doi: 10.1007/s00267-009-9335-3

Tables

Table 1: Validation of SWIM at three gauging stations in the Mulde catchment

Gauging Station	mNS	NS
Bad Dueben	0.842	0.801
Erlln	0.866	0.808
Wechselburg	0.818	0.692

Table 2: Water level evaluation in the Mulde catchment

Gauging station	Peak Error (m)	Bias (m)
Wechselburg 1	0.565	0.239
Zwickau-Poelbitz	0.304	0.212
Bad-Dueben	0.391	-0.255
Golzern 1	0.341	0.342
Erlln	0.184	-0.014

Figures

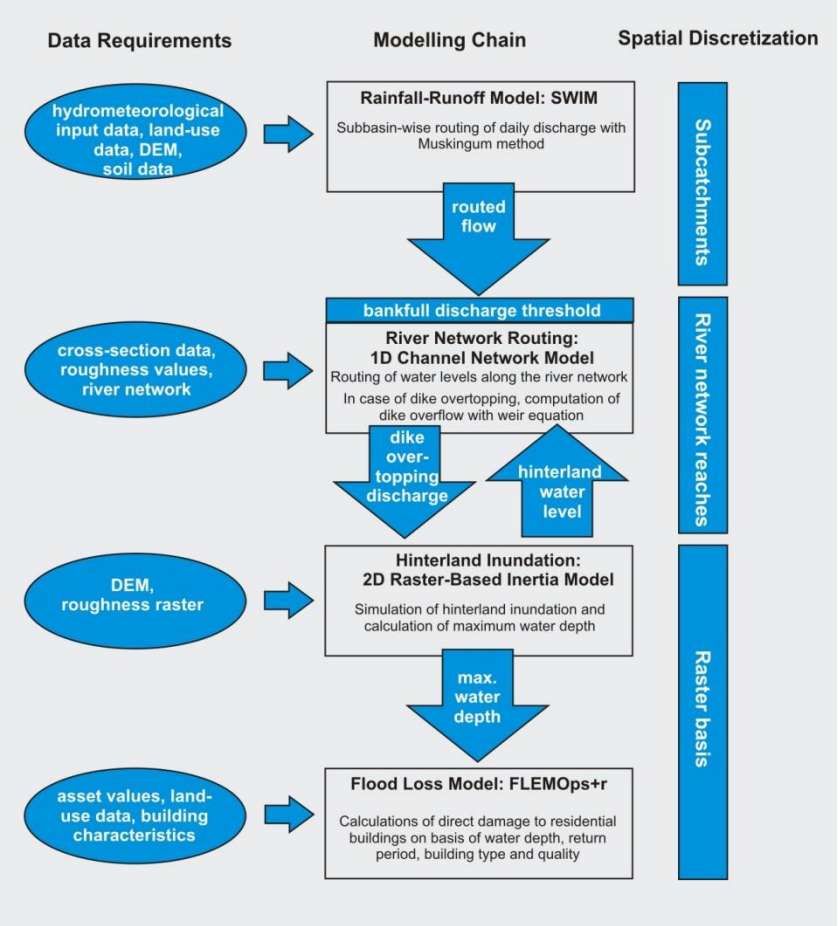

Figure 1: Components and data requirements of the Regional Flood Model (RFM). DEM, digital elevation model; FLEMOps+r, Flood Loss Estimation MOdel for the private sector; SWIM, soil and water integrated model.

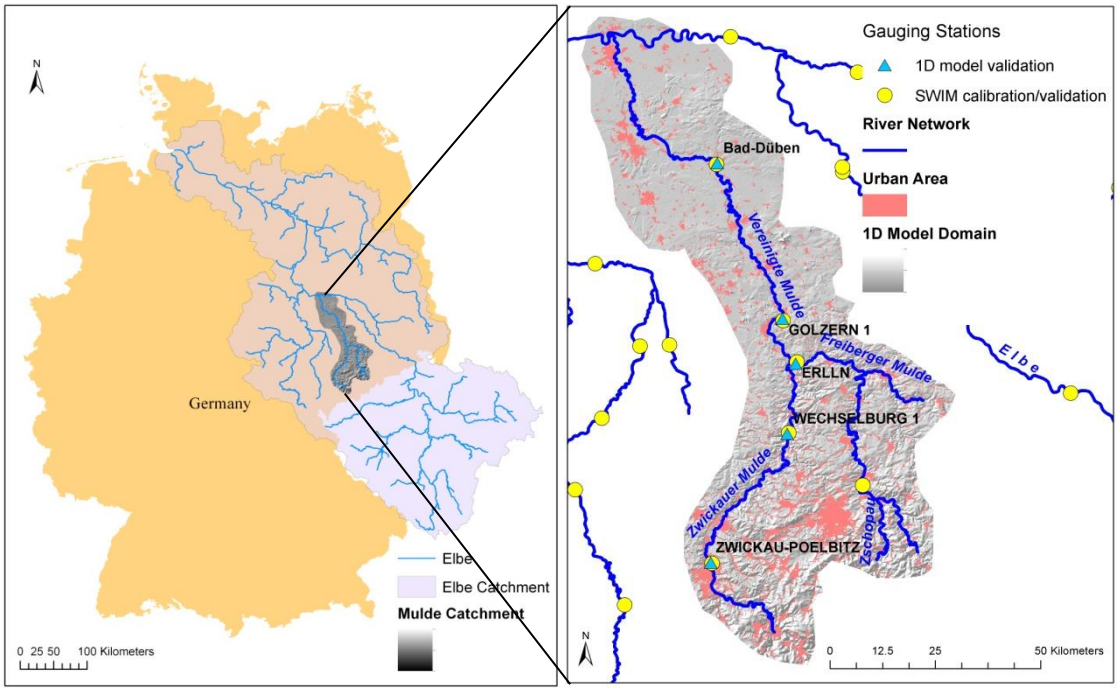

792

793 **Figure 2: Study area, left panel: overview of the entire Elbe catchment including Czech areas;**
794 **right panel: study area including the simulated river network, the 2D model domain and**
795 **locations used for model calibration and validation.**

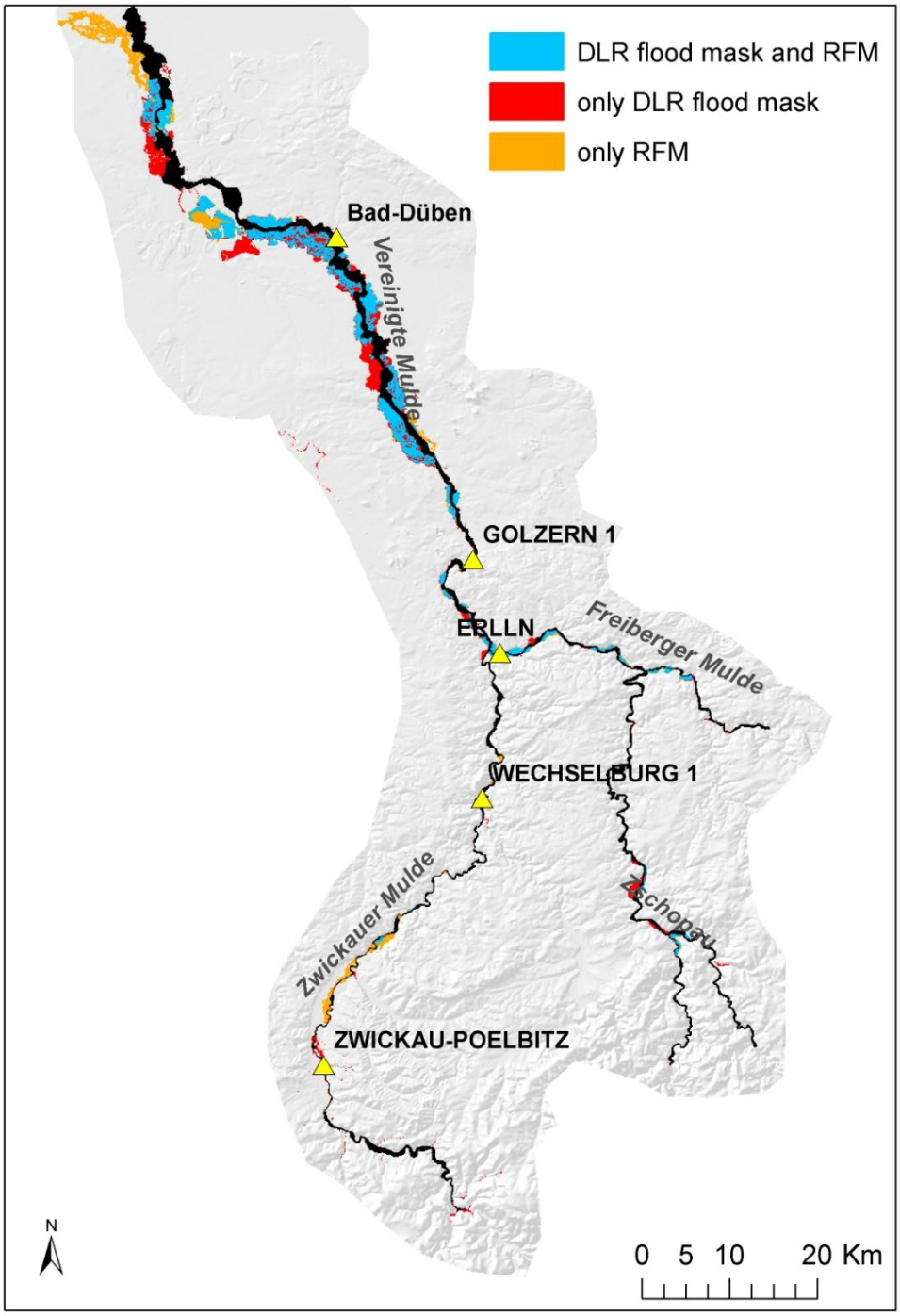

796

797 **Figure 3: Comparison of simulated and observed inundation extents for the August 2002 flood**

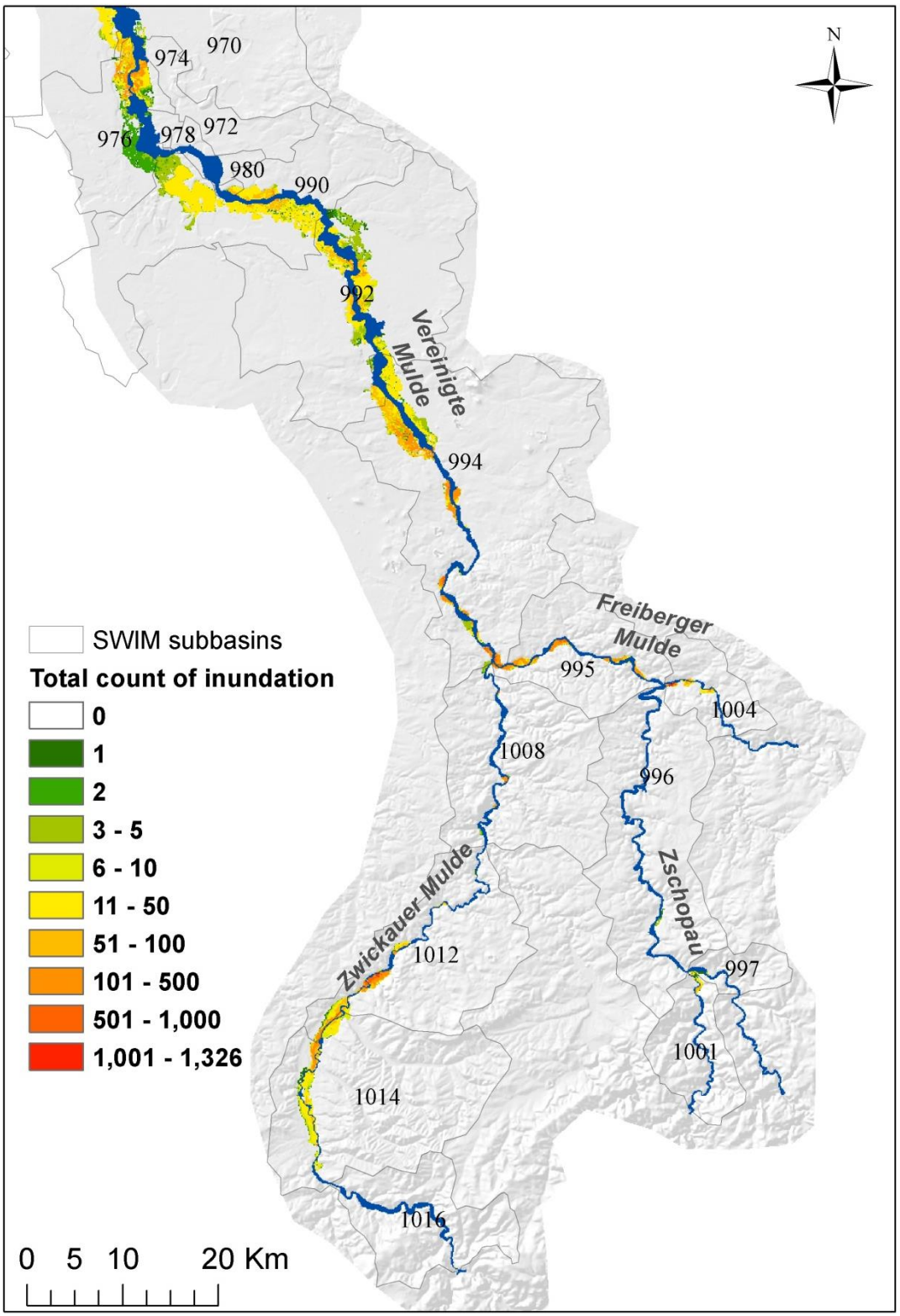

798

799 **Figure 4: Inundation frequency in 10,000 years of simulation for each computational cell**

800

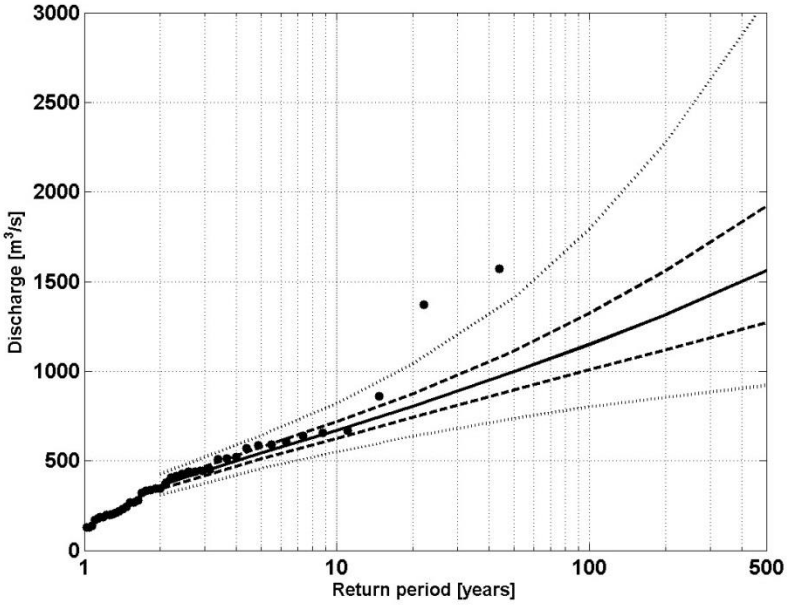

801

802 **Figure 5: Comparison of derived flood frequency curve and plotting positions for gauge Bad**
803 **Düben. Dots are the observations; the solid line is the median of the derived frequency curves;**
804 **the dashed and dotted lines show the 50% and 95% confidence interval, respectively.**

805

806

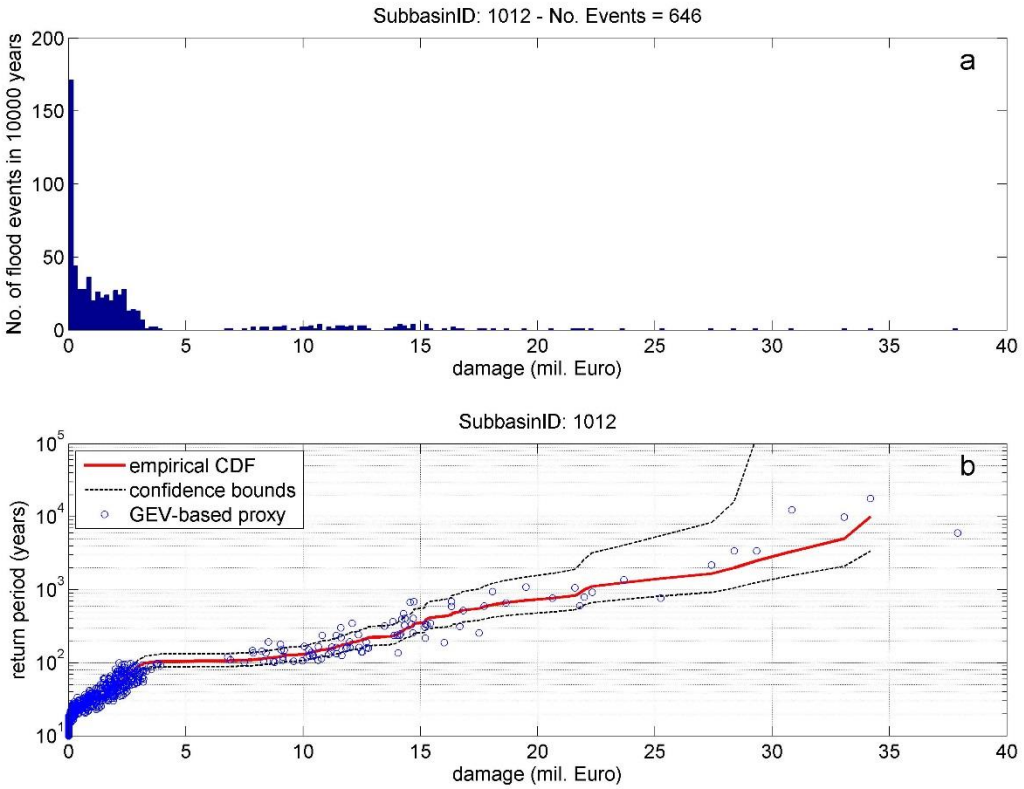

807

808 **Figure 6: (a) Histogram of damage events and (b) comparison of traditional and simulation-**

809 **based risk curves for an exemplarily subbasin.**

810

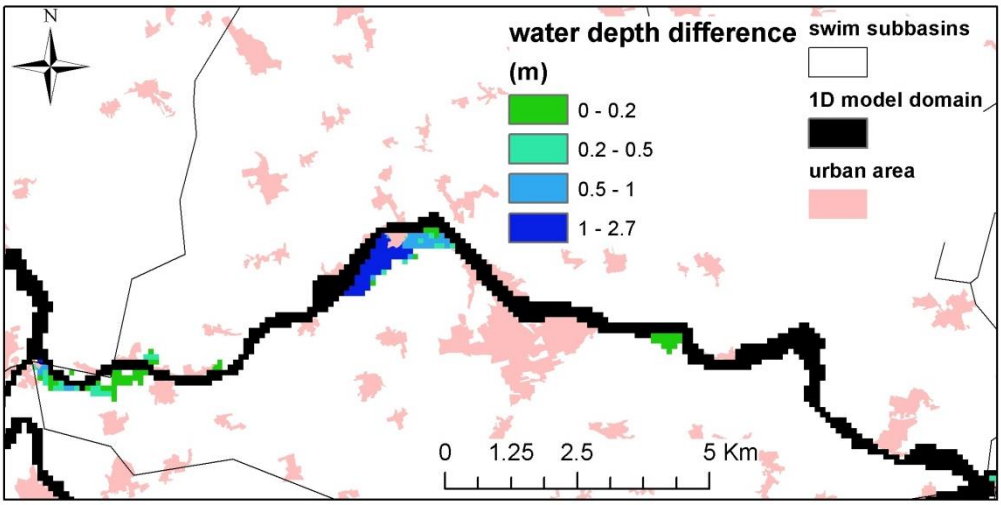

811

812

813 **Figure 7: Differences in inundation depth for two flood events with the same flood peak in**

814 **subbasin 995.**

815

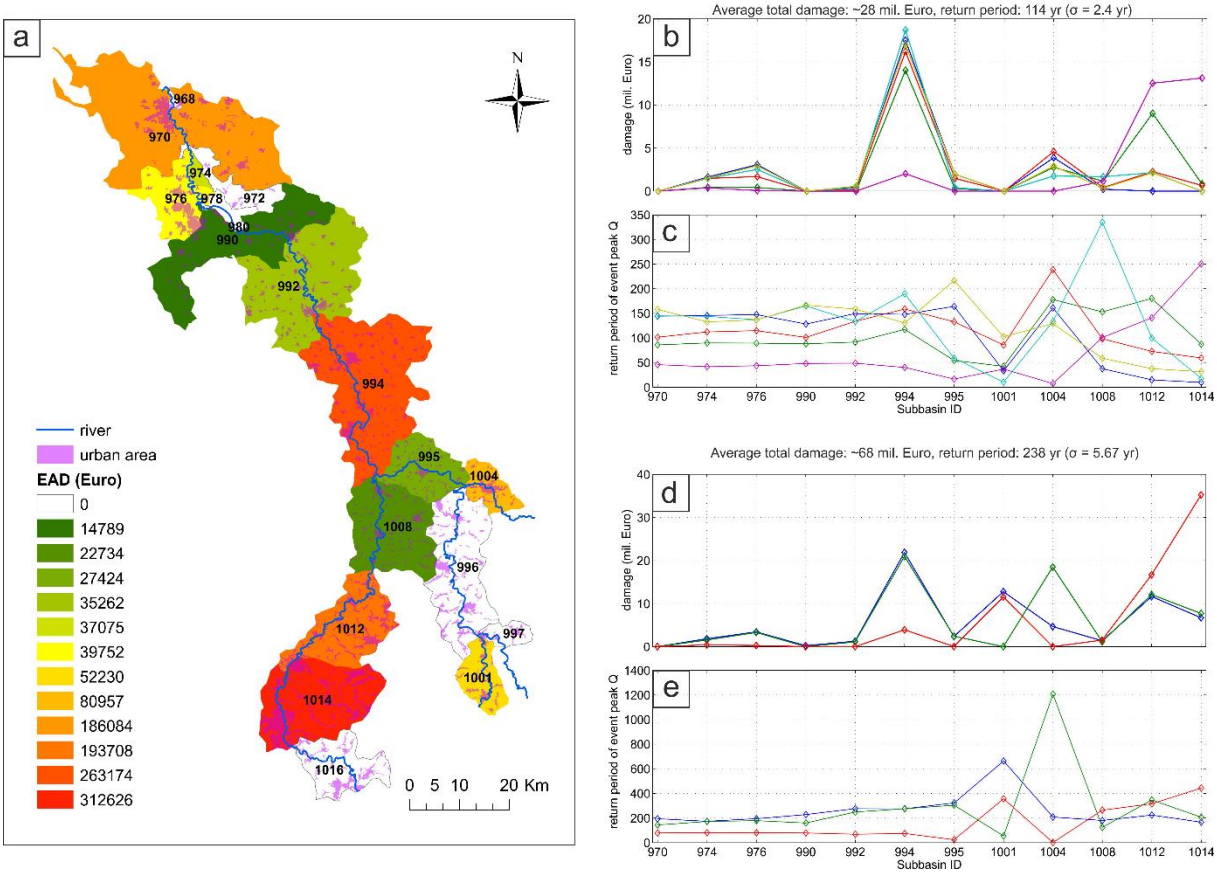

816

817 **Figure 8: a) Distribution of Expected Annual Damage to residential buildings in the Mulde**
818 **catchment at the subbasin scale. b) – e) Comparison of total damage (b, d) and discharge**
819 **return period (c, e) spatial distributions among subbasins (x-axis) and different flood events**
820 **(coloured lines) for two different levels of total catchment damage.**